Composites: Part A 186 (2024) 108382

Contents lists available at ScienceDirect

Composites Part A

journal homepage: www.elsevier.com/locate/compositesa

Multifunctional sandwich composites with optimized phase change material content for simultaneous structural and thermal performance

Giulia Fredi *, Elisa Boso, Alessandro Sorze, Alessandro Pegoretti

University of Trento, Department of Industrial Engineering and INSTM Research Unit, Via Sommarive 9, 38123 Trento, Italy

ARTICLE INFO

Keywords:
Sandwich structures
Thermal properties
Interface/interphase
Mechanical testing

ABSTRACT

This work aims at developing novel multifunctional sandwich composites with optimized thermal energy storage and structural load-bearing performance by incorporating microencapsulated phase change materials (PCMs) into polyurethane (PU) foam cores. The optimized foam containing 20 wt% PCM, balancing good latent heat storage (up to 29 J/g) with low thermal conductivity (up to 0.035 W/(m·K) at 50 °C), was used to produce sandwich panels with high-performance epoxy/carbon fiber laminate skins. Microstructural characterization confirmed excellent interfacial adhesion between the core and skins. The multifunctional panels exhibited comparable flexural strengths (150 kPa) and facing stresses (25 MPa) to neat PU sandwich controls. By integrating thermal regulation from PCM phase change with structural reinforcement from the sandwich architecture in a single multifunctional material system, this work contributes to the development of lightweight, energy-efficient composite materials suitable when weight reduction and thermal management are paramount, such as in aeronautics and cold chain logistics.

1. Introduction

Sandwich composite structures, consisting of two thin but stiff face sheets separated by a lightweight core material, have gained significant attention due to their exceptional specific stiffness and strength, especially to flexural load [1]. These properties make sandwich composites attractive for various applications, including aerospace, automotive, marine, and construction industries, where weight reduction is crucial [2]. One of the main advantages associated with sandwich structures is the availability of a diverse range of core designs and materials. Every core has its unique properties in terms of specific strength and stiffness, weight, energy absorption capability, and, ultimately, cost on the market. The core materials employed in sandwich composites can range from polymeric foams (e.g., polyurethane (PU), polyvinyl chloride (PVC), and polystyrene (PS)) to honeycomb structures (e.g., aluminum, aramid, and Nomex) and advanced core materials like balsa wood and syntactic foams [3]. Among these options, polymer foam cores, particularly PU foams, offer several advantages, including low density, ease of processing, good thermal insulation, shock wave absorption, low-velocity impact resistance, crashworthiness, and acoustic damping, making them an attractive choice for various structural applications [4].

Besides the mechanical performance, enhancing the thermal management capabilities of sandwich composite structures has emerged as an area of significant interest, driven by the growing demand for energy-efficient systems and temperature regulation in diverse applications. Up to now, the focus has primarily been on the decrease in thermal conductivity, effective in the steady state regime, while there may be an advantage in increasing the thermal inertia also with a variable heat source. This can be reached by decreasing the thermal diffusivity of the foam core, but also with the introduction of a phase change material (PCM) [5–7]. PCMs are substances capable of storing and releasing substantial amounts of latent heat during phase transitions, typically between solid and liquid states, within a narrow temperature range [8,9]. Organic solid–liquid PCMs, such as paraffin waxes and fatty acids, have gained prominence for low-to-medium-temperature thermal management applications due to their suitable phase change temperatures, high latent heat storage capacity, and chemical stability [10–12]. These characteristics have been exploited by incorporating PCMs, mostly in their microencapsulated form [13–15], in buildings via the production of PCM-enriched wallboards and concrete or gypsum panels [16,17].

The integration of PCMs into polymer foam cores, particularly PU foams, has been extensively investigated in recent years [18,19]. Numerous studies have focused on encapsulating PCMs within PU

* Corresponding author.
E-mail address: giulia.fredi@uni.tn.it (G. Fredi).

https://doi.org/10.1016/j.compositesa.2024.108382
Received 6 June 2024; Received in revised form 12 July 2024; Accepted 29 July 2024
Available online 31 July 2024

foams, producing materials with enhanced thermal energy storage (TES) and thermal buffering properties [20–25]. The introduction of PCMs into PU foams has been shown to modify the microstructure, with the PCM microcapsules influencing the cell morphology, size distribution, and overall porosity of the foam [26,27], which in turn affects their mechanical properties. Furthermore, the presence of PCMs can alter the thermal conductivity and insulation performance of the foam, leading to a complex interplay between thermal energy storage and heat transfer characteristics [21].

Although the introduction of PCM in PU foams has been largely investigated, the use of PCM-enhanced PU foams to produce structural sandwich panels has been surprisingly limited. Indeed, the existing studies of sandwich composites with a core containing PCMs primarily concentrate on non-structural applications, namely as insulating layers for cold chain containers and building envelopes [28–30]. One of the very few examples of structural sandwich panels containing PCMs is that proposed by Castellón et al. [5], who developed a structural panel by foaming a PCM-enriched rigid PU foam between two metal sheets. Although this work proved the effectiveness of such a design concept from the thermal point of view, the mechanical characterization of the foam and the panel is completely missing. Hence, the development and the all-round characterization of such sandwich panels containing PCMs is a research gap that is yet to be filled.

In fact, the incorporation of PCMs into structural composites presents an appealing multifunctional concept that simultaneously addresses load-bearing and thermal energy storage requirements [31–33] and has the potential to effectively fill this research gap. Our group has explored this concept by developing polymer matrix composites reinforced with continuous and discontinuous fibers and other types of fillers [34–37]. The obtained results suggested that integrating PCMs within the core of sandwich composite structures may confer an advantage by combining the latent heat storage capability of PCMs with the exceptional specific strength and stiffness inherent to sandwich designs. This may allow considerable mass and volume saving at the component level compared to juxtaposing material performing only the structural function to another contributing solely to the thermal management. This approach facilitates the development of lightweight, energy-efficient composites capable of meeting the stringent demands for thermal management and mechanical robustness in various applications, such as the automotive, aerospace, and refrigerated transportation fields [28,38–40]. For example, the developed sandwich composites could find particularly valuable application in the refrigerated transportation of temperature-sensitive goods like pharmaceuticals or perishable foods. In this context, these materials could be used to construct the walls and ceiling of refrigerated truck trailers or shipping containers. The structural properties of the sandwich panels would provide the necessary strength and stiffness to withstand the mechanical loads during transportation, while simultaneously offering improved thermal management. The PCM within the foam core would act as a thermal buffer, absorbing heat during temporary rises in external temperature (e.g., when the trailer doors are opened for loading/unloading) and releasing it when the temperature drops, thus helping to maintain a more stable internal temperature. This thermal stability is crucial for preserving the quality and safety of temperature-sensitive cargo. Moreover, the enhanced thermal performance could potentially reduce the energy consumption of the refrigeration system, leading to fuel savings and decreased environmental impact. Therefore, by strategically utilizing PCM-enhanced cores in sandwich composites, the necessity for separate structural and thermal management units can be circumvented, thereby enabling significant mass and volume savings at the system level [32].

Hence, to exploit the known advantages of PCM-enhanced PU foams and fill the mechanical property gap that prevents their extensive use in structural applications, this work proposes, for the first time, the development and comprehensive characterization of a novel sandwich composite system combining the advantages of PU/PCM foams as the core material and high-performance epoxy/carbon fiber laminates as the structural skins. Although the production of PU-PCM foams has been already discussed in the scientific literature, the role of such foams as a multifunctional core in structural sandwich panels combining mechanical and thermal properties has never been reported and represents the novelty of this work. By optimizing the PCM content within the PU foam core, this multifunctional composite aims to strike an optimal balance between mechanical properties, crucial for structural applications, and thermal management capabilities facilitated by the latent heat storage of the PCM. The research methodology employed in this study involves three subsequent steps. First, PU foams containing various fractions of microencapsulated PCMs were produced and characterized with a PCM content of up to 30 wt%, to identify the optimal composition. Then, sandwich panels were fabricated by using the selected PU/PCM foam as the core material and epoxy/carbon fiber laminates as the skins. Finally, the produced panels underwent a comprehensive characterization, encompassing microstructural, thermal, and mechanical analyses. Particular emphasis was placed on evaluating the effects of PCM incorporation on the skin/core adhesion and the failure mechanisms under various loading conditions, including flexural, edgewise compression, and flatwise tensile loading.

2. Materials and methods

The methodology followed in this paper is schematized in Fig. 1.

2.1. Materials

For the preparation of the sandwich cores, polyol HDR R 150 (viscosity at 23 °C=1050 mPa•s; density at 23 °C=1.1 g/cm^3) and isocyanate ISN 1 (viscosity at 23 °C=200 mPa•s; density at 23 °C=1.23 g/cm^3) were both provided by Kairos Srl (Verona, Italy). As suggested by the producer's datasheet, PU foams for the sandwich cores were produced by mixing polyol and isocyanate in a ratio of 100:130. MPCM 32D® microencapsulated phase change material was supplied by Microtek Laboratories Inc. (OH, USA) in the form of a dry powder with a mean particle size of 15–30 μm, a density of 0.9 g/cm^3, a nominal melting point of 32 ± 2 °C, and a latent heat of fusion of 160 J/g.

For the preparation of the epoxy/carbon sandwich skins, the epoxy base Elan-tech® EC 152 (viscosity at 25 °C=1200–1800 mPa•s) and the hardener Elan-tech® W 152 MR (viscosity at 25 °C=30–60 mPa•s) were kindly provided by Elantas Europe Srl (Parma, Italy) and mixed at a ratio 100:30, as recommended on the producer's datasheet. Balanced plain weave carbon fabric Angeloni GG 200P (mass per unit area = 192 g/cm^3) was supplied by G. Angeloni Srl (Venezia, Italy).

2.2. Sample preparation

2.2.1. Preparation of foam samples

First, the required amounts of polyol and isocyanate were weighed and poured into separate beakers. For the PCM-containing compositions, the necessary PCM mass was weighed and split equally into the two beakers. Primary mixing by hand was then performed in each beaker using a spatula. Then, the content of the two beakers was combined, mechanically mixed for approx. 25–30 s, and then poured into a mold with an inner cavity of 250 × 250 × 20 mm3, preheated at 40 °C. The mold was lined internally with PTFE sheets and polyethylene film to facilitate sample extraction. The mold was rapidly covered and cured in an oven at 40 °C for 20 min. Appropriate clamping was applied to counteract the pressure developed during crosslinking and foaming. After the first 15 min, the cover was removed, and the mold was left open to complete curing. The preparation was repeated for both neat and PCM-containing PU foams, and at least two specimens were prepared for each composition. The prepared foams with the nominal weight compositions are listed in Table 1.

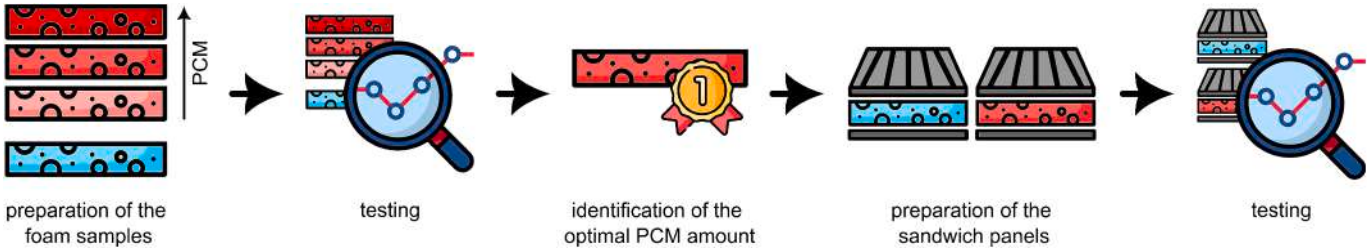

Fig. 1. Scheme of the methodology followed in this work.

Table 1
List of the prepared samples with nominal composition.

Foam samples	Polyol + isocyanate (wt%)	PCM (wt%)
PU	100	0
PU-PCM10	90	10
PU-PCM20	80	20
PU-PCM30	70	30
Sandwich panels	Core	Skin
S-PU	PU	Epoxy/carbon laminate
S-PU-PCM20	PU-PCM20	Epoxy/carbon laminate

2.2.2. Preparation of sandwich panels

After the characterization of the foams, the sample PU-PCM20 presented an optimal balance between thermal and mechanical properties. Hence, composite sandwich panels were prepared with either neat PU or PU-PCM20 core materials (Table 1). After production, the foams were milled on both surfaces to remove the thin, denser layer on the outer surface and to reach the desired size of 200 × 200 × 15 mm^3. Then, sandwich panels were prepared by hand layup and vacuum bagging. Three carbon fiber (CF) laminae were impregnated with the epoxy/hardener mixture and placed on the top of a flat steel plate. Then, the foam panel was placed onto them, and finally, three more CF laminae were added on top, each one of them impregnated with the epoxy/hardener mixture. During stacking, both surfaces of the foam were wet with additional epoxy/hardener mixture, to ensure a proper interfacial adhesion. The vacuum bag was then sealed, and the composite was left curing under vacuum for 24 h at room temperature. Each sandwich panel was then demolded and post-cured at 60 °C for 15 h, as recommended by the epoxy resin producer's datasheet. Two specimens were produced with the neat PU foam as a core and two additional specimens with the PU-PCM20 foam.

2.3. Characterization

2.3.1. Characterization of the foam samples

Microstructural characterization. Scanning electron microscopy (SEM) was performed to characterize the microstructure of the prepared foam samples. The specimens were cryofractured, coated with Pt-Pd, and observed with a Zeiss Supra 40 (Carl Zeiss AG, Oberkochen, Germany) field emission scanning electron microscope (FE-SEM) operating at an accelerating voltage of 3.5 kV. The SEM micrographs were analyzed to measure the cell size distribution via the software ImageJ.

The density of the prepared foams was measured to calculate the total, open, and closed porosity as a function of the PCM concentration. This calculation required the evaluation of the theoretical density (ρ_{th}) of a PU sample without porosity, the apparent density (ρ_{app}), identifying the solid wall volume together with only the closed porosity, and the bulk density (ρ_{bulk}), comprising both the open and the closed porosity. ρ_{th} was evaluated with the rule of mixture, by knowing the densities and the nominal weight fractions of each constituent. Since the theoretical density of neat PU without pores is very difficult to obtain experimentally, because the production of a void-free PU sample is not feasible with the reagents used in this work, the density of the liquid precursors was used for the calculation. The authors are well aware that the density of solid PU cell walls can be quite different from the linear combination of the density of its precursors, but this was the only method allowing us to obtain a reliable value for ρ_{th}, fundamental to quantify the porosity value. Hence, ρ_{th} was calculated via Eq. (1) as

$$\rho_{th} = \frac{1}{\sum_i \frac{W_i}{\rho_i}} = \frac{1}{\frac{W_{pol}}{\rho_{pol}} + \frac{W_{iso}}{\rho_{iso}} + \frac{W_{PCM}}{\rho_{PCM}}} \quad (1)$$

where W_{pol}, W_{iso}, and W_{PCM} are the weight fractions of the polyol, the isocyanate, and the PCM, respectively, and ρ_{pol}, ρ_{iso}, and ρ_{PCM} their densities. ρ_{pol} and ρ_{iso} were found on the technical datasheet (see Section 2.1), while ρ_{PCM} was measured with a pycnometer, as reported hereafter for the apparent density.

The apparent density (ρ_{app}) was measured using an AccuPyc 1330 helium pycnometer (Micromeritics Instrument Corporation, GA, USA). For every composition, a cylindrical specimen with a diameter of approx. 8 mm was cut out of the foam and inserted in a chamber with a volume of 1 cm^3. Specimens were extracted from the inner part of the original foam specimen, excluding the outer, dense skins. Every measurement was collected at a constant temperature of 23 °C, and 99 measurements were performed for each specimen.

The bulk density (ρ_{bulk}) was calculated as the ratio between the mass and the volume of prismatic specimens with nominal dimensions of 15 × 15 × 25 mm^3. The dimensions of the specimens were measured with a digital caliper and the mass with an analytical balance. Three specimens were measured for each composition.

Then, the total porosity ($\varnothing_{tot}$), the open porosity ($\varnothing_{open}$), and the closed porosity ($\varnothing_{closed}$) were calculated via Eq. (2), as

$$\varnothing_{tot} = 1 - \frac{\rho_{bulk}}{\rho_{th}} \quad (2)$$

$$\varnothing_{open} = 1 - \frac{\rho_{bulk}}{\rho_{app}} \quad (3)$$

$$\varnothing_{closed} = \varnothing_{tot} - \varnothing_{open} = \rho_{bulk}\left(\frac{1}{\rho_{app}} - \frac{1}{\rho_{th}}\right) \quad (4)$$

Thermal characterization. Thermogravimetric analysis (TGA) was performed via the IR thermobalance Mettler TG 50 (Mettler Toledo Inc., Columbus, Ohio, USA). Specimens of approx. 20 mg were subjected to a thermal ramp between 30 °C and 700 °C with a heating rate of 10 °C/min, under a constant nitrogen flow of 10 ml/min. This test allowed the determination of the temperatures corresponding to a mass loss of 1 wt %, 3 wt%, and 5 wt% ($T_{1\%}$, $T_{3\%}$, $T_{5\%}$), and the degradation temperature (T_d), at the maximum of the first derivative of the TGA thermogram (DTG), and the residual mass at 700 °C ($m_{R,700}$).

Differential scanning calorimetry (DSC) was performed via a Mettler DSC 30 (Mettler Toledo Inc., Columbus, Ohio, USA). Specimens of approx. 10 mg were sealed in aluminum crucibles and subjected to a heating/cooling/heating cycle between −50 °C to 100 °C at ± 10 °C/min, under a constant nitrogen flow of 100 ml/min. The tests allowed measuring the melting and crystallization temperatures (T_m and T_c) and enthalpies (ΔH_m and ΔH_c) of the PCM contained in the foams. From the

enthalpy values, the relative enthalpy (ΔH_{rel}) was calculated for each sample and each of the three DSC scans through Eq. (5), as

$$\Delta H_{rel} = \frac{\Delta H_{exp}}{\Delta H_{PCM}\hat{A}\cdot W_{PCM}} \quad (5)$$

where ΔH_{exp} and ΔH_{PCM} are the melting or crystallization enthalpies experimentally measured on foam samples and on neat PCM, respectively, and W_{PCM} is the nominal PCM concentration in each sample. Hence, $\Delta H_{PCM}\hat{A}\cdot W_{PCM}$ is a measurement of the theoretical enthalpy each sample would have developed if no PCM was lost or damaged in the process.

Thermal conductivity tests were performed on specimens of 200 × 200 × 20 mm^3 with a heat flow meter HFM 446 Lambda (Netzsch Gmbh, Selb, Germany), at mean temperatures of 10 °C (i.e., with solid PCM), 30 °C, and 50 °C (i.e., with melted PCM), with a temperature difference between the specimen sides of 20 °C.

The thermal behavior of the foams was also analyzed with the FLIR E6 IR thermal imaging camera (Teledyne FLIR llc, NH, USA), to evaluate the thermal management capability of the foams on a sample bigger than that evaluated with DSC. The test was performed in two configurations, i.e., under heating and cooling conditions. For the experiment under heating conditions, the specimens were conditioned at −18 °C for at least 12 h and then placed in an oven at 50 °C and left heating while the surface temperature was recorded with the thermal camera. For the experiment under cooling conditions, the specimens were conditioned at 70 °C for at least 12 h and then placed at 10 °C and left cooling while the surface temperature was recorded with the thermal camera. The goal of such a procedure was to evaluate how the PCM influenced the heating and cooling speeds. The test was performed on one specimen per composition, with dimensions 200 × 200 × 20 mm^3. The emissivity of the material was set to 0.96.

Dynamic mechanical thermal analysis (DMTA) was performed with the TA Q800 DMA instrument (TA Instruments, New Castle, DE, USA). Tests were carried out in single cantilever mode on rectangular specimens with nominal dimensions of 30 × 12 × 6 mm^3, mounted on grips with a free length of 17.5 mm. The storage modulus (E'), loss modulus (E''), and loss factor ($tan\delta$) were measured as a function of temperature from −50 °C to 140 °C, with a 3 °C/min heating rate and an applied strain of 0.05 % at a frequency of 1 Hz. The tests were performed both on the as-prepared samples and on samples treated at 200 °C for 30 min to complete the polymer curing. The DMTA was therefore also focused on investigating the effects of such treatment.

Mechanical characterization. Mechanical testing was performed with an Instron 5969 universal testing machine (Instron, Norwood, MA, USA), equipped with a 1-kN load cell and a thermal chamber allowing measurements at different temperatures. Three-point flexural and uniaxial compression tests were performed for each sample composition at 20 °C and 40 °C, i.e., below and above the melting temperature of the PCM.

Three-point flexural tests were performed according to the standard ISO 1209–2:2004, on specimens with nominal dimensions of 200 × 20 × 10 mm^3, with a span length of 120 mm and a crosshead speed of 20 mm/min. Five specimens were tested for each composition at each testing temperature. The test allowed the measurement of the flexural modulus (E_f), flexural strength (R_f), and strain at maximum load (ε_{Rf}).

Compression tests were performed following the standard ASTM D1621-16, on specimens with nominal dimensions of 50 × 50 × 20 mm^3, with a crosshead speed of 2 mm/min (i.e., 10 % of the specimen height, according to the standard). Five specimens were tested for each composition at each testing temperature. The test allowed the measurement of the compressive modulus (E_c) and compressive strength (R_c). More specifically, R_c was calculated as the yield stress, if yielding occurred at strains of less than 10 %, or as the stress at 10 % strain, in the other cases.

Statistical analyses were performed using R Studio version 2023.12.1 (RStudio, Inc., Boston, MA, USA). To assess the effects of the experimental factors (composition and testing temperature) and their potential interaction, a two-way analysis of variance (ANOVA) was conducted. In cases where the ANOVA revealed statistically significant differences, Tukey's honest significant difference (HSD) post-hoc test was employed to identify specific group comparisons that were significantly different from one another. All statistical tests were evaluated at a significance level of 0.05.

2.3.2. Characterization of the sandwich panels

Microstructural characterization. Light microscopy (LM) was performed to qualitatively assess the core-skin interfacial adhesion. Samples were embedded in epoxy resin, polished with polishing papers, and observed with a Zeiss AXIO Imager.A1m optical microscope (Carl Zeiss AG, Oberkochen, Germany) at different magnification levels. Both the top and bottom skins were observed in this way.

Thermal characterization. DSC tests were performed on the skins of the sandwich panels to measure the glass transition temperature of the cured epoxy resin, so to evaluate the applied curing cycle. DSC scans were performed with the same equipment and testing parameters described above for the foam characterization. The test was performed on specimens from all the prepared panels, taken from the top and the bottom skins.

TGA tests were also performed on the skins, to assess the mass composition and the fiber volume fraction. The tests were performed with the same equipment and testing parameters described above for the foam characterization. The test was also performed on a sample of neat epoxy resin cured in the same way as the skins of the sandwich panels. The comparison between the residual mass after the test ($m_{R,700}$) of the skins and the neat epoxy resin allowed the determination of the mass composition of the skins, and specifically of the fiber mass fraction ($W_{f,TGA}$). The fiber mass fraction determined in this way was compared with that determined by weighing the foam core and the carbon fibers before the hand layup process and the final sandwich panel after hand layup. The mass difference, all attributable to the added epoxy resin, allowed the calculation of the mass composition of the carbon/epoxy skins, and specifically of the fiber mass fraction ($W_{f,wm}$). In both cases, the fiber volume fraction was then calculated via the mixture rule by knowing the mass fraction of matrix and fibers and their densities, measured by helium pycnometry at 23 °C, which led to the calculation of the fiber volume fraction in the composite skins with the two methods ($V_{f,wm}$, $V_{f,TGA}$). This calculation was done by neglecting the volume fraction of voids, which was set equal to zero. The authors understand this assumption leads to an overestimation of the fiber volume fraction determined in this way.

Thermal conductivity tests were carried out using the HFM machine described for the foam samples, equipped with a specific instrumental kit for testing rigid materials. As for the foams, three tests were performed for each specimen by changing the temperature applied on the top and bottom sides, to reach average temperatures of 10 °C, 30 °C, and 50 °C, with a temperature difference between the specimen sides of 20 °C. The analysis not only helped quantify the effect of conductive epoxy/carbon skins but also that of the possible penetration of epoxy in the open foam porosity on the overall insulation performance.

Mechanical characterization. The mechanical characterization, carried out at 20 °C with the same testing machine described for the foams, involved three-point flexural, edgewise compression, and flatwise tensile tests. The used load cell was a 10-kN cell for the first two tests and a 1-kN cell for the third.

Three-point flexural tests were conducted according to the ASTM C393/C393M-20 standard, on six specimens per sample with nominal dimensions of 200 × 30 × 15 mm^3, with a span length of 150 mm and a crosshead speed of 3 mm/min. From the recorded load–displacement curves, the core shear ultimate strength (σ_s^{ult}) was calculated as in Eq. (6),

$$\sigma_s^{ult} = \frac{P_{max}}{(d+c)\hat{A}\cdot b} \tag{6}$$

where P_{max} is the maximum load observed before failure, d is the sandwich thickness, c is the core thickness, and b is the specimen width. Moreover, the bending stress observed in the facings at the maximum applied load, denoted as facing stress (σ_{fac}), was also determined as in Eq. (7), as

$$\sigma_{fac} = \frac{S\hat{A}\cdot P_{max}}{2t\hat{A}\cdot(d+c)\hat{A}\cdot b} \tag{7}$$

where S is the span length and t is the facing thickness, calculated as $(d-c)/2$.

Edgewise compression tests were performed according to the ASTM C364/C364M-16 standard on six rectangular specimens per sample with nominal dimensions of $60 \times 50 \times 15$ mm^3. The specimens were oriented so that the uniaxial compressive load was applied parallel to the laminate plane on a cross-sectional area of 50×15 mm^2. The crosshead speed was fixed at 0.75 mm/min. From the load–displacement curves, the ultimate edgewise compressive strength (σ_{ec}^{ult}) was determined according to Eq. (8), as

$$\sigma_{ec}^{ult} = \frac{P_{max}}{2t_{fs}\hat{A}\cdot w} \tag{8}$$

where P_{max} is the maximum load before failure, t_{fs} is the face sheet thickness, calculated as half of the difference between the sandwich thickness and the core thickness, and w is the specimen width. Moreover, the analysis focused on determining the residual mechanical strength of the sandwich structure loaded by edgewise compression after the first failure. For this purpose, two out of six specimens for both foam compositions were tested by applying the compressive load until the first damage occurred, unloading the specimen immediately after the failure to recover the deformation, and applying the compressive load again, to evaluate the residual mechanical strength.

Finally, flatwise tensile tests were carried out according to the ASTM C297/C297M-16 standard on six specimens per sample with nominal dimensions of $25 \times 25 \times 15$ mm^3. The uniaxial tensile load was applied in the direction orthogonal to the laminate skins, trying to separate the core from the face sheets. This aimed at evaluating the core-skin adhesive strength. The crosshead speed was fixed to 0.5 mm/min. From the recorded load–displacement curves, the ultimate flatwise tensile strength (σ_t^{ult}) was calculated via Eq. (9), as

$$\sigma_t^{ult} = \frac{P_{max}}{A} \tag{9}$$

where P_{max} is the maximum load before failure and A is the cross-sectional area.

The mechanical results were statistically treated using R Studio v. 2023.12.1 (RStudio, Inc., Boston, MA, USA). A one-way analysis of variance (ANOVA) was conducted to assess the effect of the composition on the various mechanical parameters. Differences were considered significant with a p-value lower than 0.05.

3. Results and discussion

This section will first present the results of the characterization of the PU foam samples with a variable amount of PCM (10, 20, or 30 wt%), which allowed the identification of the foam PU-PCM20 as that featuring an optimal combination of thermal and mechanical properties. The second part of this section will be devoted to present the results of the characterization of the sandwich panel having a PU-PCM20 core, benchmarked against the sandwich panel with a neat PU core.

3.1. Characterization of the foam samples

3.1.1. Microstructural properties of the foam samples

The microstructural characterization of the foam samples revealed significant modifications in cell shape and size with increasing PCM content (Fig. 2a–h). The neat PU foam (Fig. 2a) exhibits the typical polyhedral closed-cell structure characterized by pentagonal or hexagonal cells, which regulates the foam's thermal and mechanical properties [41,42]. As the PCM content increases, the cell shape is transformed from polyhedral to more spherical, and the cell dimensions appear to decrease (Fig. 2b), due to nucleation effects as explained later. At higher PCM loadings, substantial changes in the cell structure are observed, transitioning from a closed-cell to an open-cell configuration. This transition is facilitated by the rupture of struts between adjacent cells promoted by the accumulation of the PCMs in the cell walls, which extensively deforms the original cell shape. The strut rupture mechanism is primarily responsible for the formation of very large cells at higher PCM contents (Fig. 2e,f). This phenomenon is further evidenced by higher magnification micrographs, which reveal that the microcapsules are preferentially located at the interface between adjacent cells. The cell struts and walls change from smooth to rough, indicating that the PCM is primarily incorporated in these regions rather than inside the cells.

In most cases, the PCM shell is observed to detach from the fractured surface, suggesting poor adhesion between the capsules and the PU foam matrix. This poor adhesion can detrimentally affect the mechanical behavior by impairing the load transfer from the polymer matrix to the capsules. However, instances are observed where the capsule shells remain attached to the matrix, indicating that the bonds are strong enough to induce crack propagation through the microcapsule. For a more detailed microstructural investigation of the PCM microcapsules themselves, the reader is suggested referring to previously published literature from our group, describing very similar microencapsulated PCM products only differing in the core's melting temperature [43–47].

The analysis of the average cell size and distribution (Fig. 2i) reveals that the mean cell diameter ranges between 200 μm and 500 μm for all foam compositions, consistently with previous studies on PU foams [18,48]. The addition of 10 wt% and 20 wt% PCM appeared to decrease the mean cell size compared to the neat PU foam, attributable to the nucleation effect promoted by the microcapsules [26,49]. However, the same result is not observed with 30 % PCM content, where strut rupture and degradation are dominant and the main effect of this is a broadening of the cell size distribution.

This cell opening effect promoted by the PCM is responsible for the density and porosity trends represented in Fig. 2j,k. The apparent and bulk densities are observed to increase with the PCM concentration, which is attributed to the PCM weakening the cell walls and promoting the transformation into an open-cell structure, as evidenced by the micrographs. In fact, the volume fraction of closed cells decreases from approx. 30 vol% of neat PU down to approx. 3 vol% of PU-PCM30, and the addition of 30 wt% PCM causes an increase in the open porosity of approx. 32 % compared to neat PU. In summary, the addition of PCM to the PU foam influences the cell structure, resulting in a decrease in total porosity, an increase in open porosity, and a reduction in the volume fraction of closed cells. These microstructural modifications significantly impact the foam's thermal and mechanical properties [50], as described in the next sections.

3.1.2. Thermal properties of the foam samples

The results of the TGA tests are reported in Figure S1 and Table S1. The PCM exhibits a higher degradation onset temperature compared to the PU foam. The PCM undergoes complete degradation before reaching 700 °C, while the PUFs experience mass reduction from the early stages of the thermal cycle but do not degrade entirely within the explored temperature range, leaving a considerable residue at 700 °C. The degradation thermograms indicate that the degradation of PU foam is

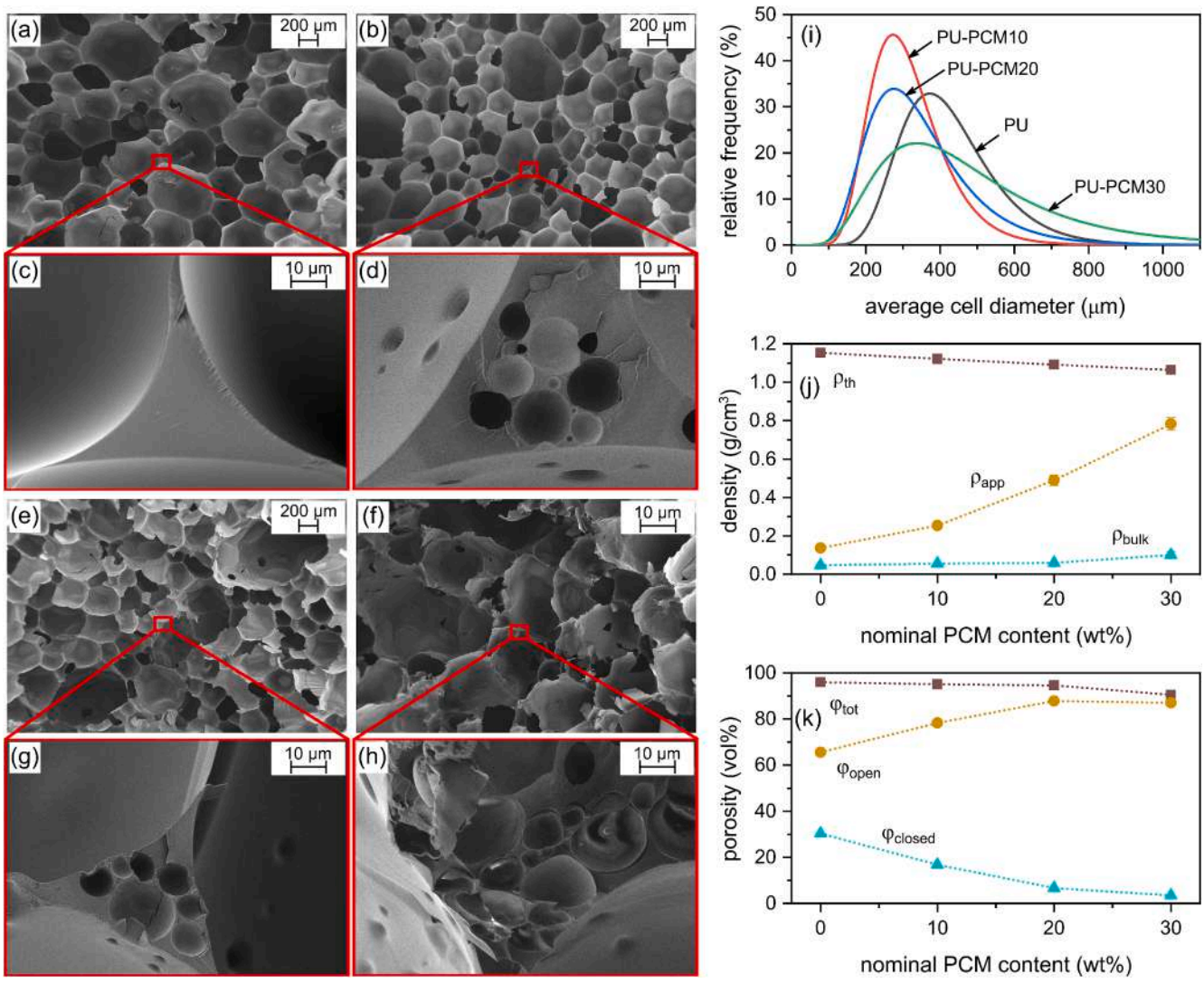

Fig. 2. Microstructural and physical characterization of the prepared foams. (a-h) SEM micrographs of the cryofracture surface of the samples (a,c) PU; (b,d) PU-PCM10; (e,g) PU-PCM20; (f,h) PU-PCM30; (i) Log-normal fit of the average foam cell size distribution obtained from the analysis of the SEM micrographs of foam samples; (j) theoretical, apparent, and bulk density of the prepared foams as a function of the PCM concentration; (k) total, open, and closed porosity of the prepared foams as a function of the PCM concentration.

the dominant mechanism for all the prepared foams, occurring with the maximum rate at a temperature more than 50 °C lower than that of the PCM.

Regarding the onset of mass reduction, the values of $T_{1\%}$, $T_{3\%}$, and $T_{5\%}$ evidence that the neat PU and PU-PCM10 samples start degrading at lower temperatures, with a $T_{1\%}$ of 53 °C and 66 °C, respectively, which may be connected to the degradation of low molecular weight compounds residual from an incomplete curing of PU. This effect is partially mitigated in PU-PCM20 and PU-PCM30, for which the beginning of the thermal degradation is shifted to slightly higher temperatures. This may be associated with a higher degree of crosslinking of the PCM-containing foams or simply be the result of the lower weight fraction of PU foam in the samples. The same effect of retardation of the thermal degradation is also observed for the degradation temperature T_d, although to a lesser extent.

The PCM undergoes complete degradation during the thermal treatment, whereas a final pyrolyzed ash content of approximately 10 % remains for all foam compositions. Although an increase in PCM content is expected to decrease the final residuals due to the lower mass fraction of PU, this trend is not observed. A possible explanation lies in the high crosslinking density of the foam, preserved with the addition of microcapsules (as suggested by the increasing glass transition temperature measured by DMTA, see Figure S2 and. Table S2), which facilitates the formation of a carbonaceous charred layer covering the PCM and impeding its further degradation [20].

Importantly, regardless of the PCM content, less than 3 % of the initial mass is lost at 100 °C, and a 5 % loss occurs only at temperatures higher than 160 °C. Since the targeted applications for thermal energy storage will likely expose the produced foams to temperature conditions that intersect with the PCM melting range, the observed thermal degradation trends are compatible with the most common target applications.

The DSC results reported in Fig. 3 and Table 2 reveal that the neat PU foam does not exhibit any evident transition in the analyzed temperature range. However, all PU-PCM samples display signals attributable to the melting/crystallization process of the PCM. Two well-separated peaks are observed in both heating and cooling scans, which may arise from the molecular weight distribution of the paraffin wax and the rotator phase transition of n-alkanes [51]. As the PCM content increases from 10 wt% to 30 wt%, the specific enthalpy stored during heating increases from 14.5 J/g to 42.0 J/g, thus confirming an improved TES capability with higher PCM loading. However, the relative melting and

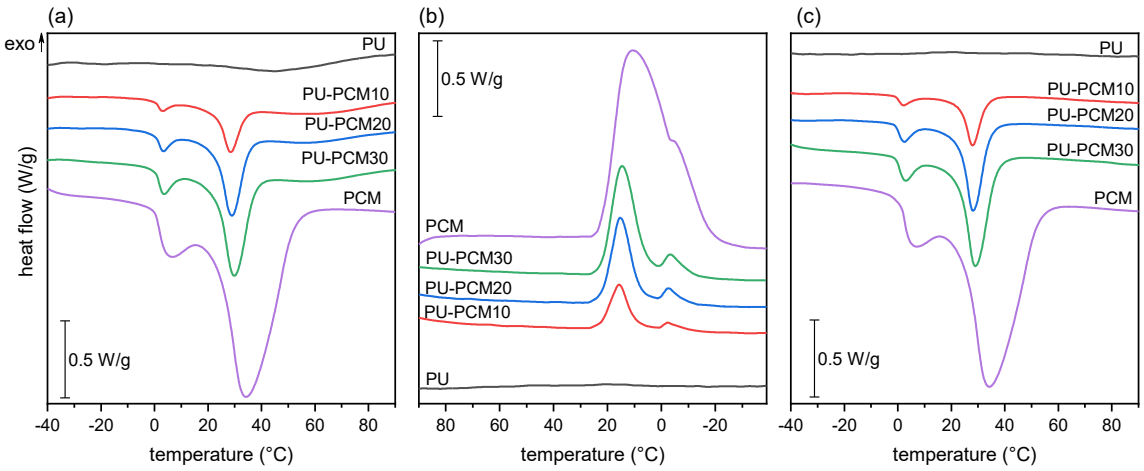

Fig. 3. DSC thermograms of the prepared foam samples. (a) First heating scan; (b) cooling scan; (c) second heating scan.

Table 2
Main results of the DSC tests on the prepared foam samples.

Sample	T_{m1}(°C)	ΔH_{m1}(J/g)	T_c (°C)	ΔH_c(J/g)	T_{m2}(°C)	ΔH_{m2}(J/g)	$\Delta H_{rel,m1}$(%)	$\Delta H_{rel,c}$(%)	$\Delta H_{rel,m2}$(%)
PU	n.a.	n.a.	n.a.	n.a.	n.a.	n.a.	n.a.	n.a.	n.a.
PU-PCM10	28.5	14.5	15.7	15.3	27.8	14.7	82.6	86.4	82.8
PU-PCM20	28.9	28.7	15.3	29.7	28.1	29.1	81.8	84.0	82.2
PU-PCM30	29.8	42.0	14.5	44.4	29	42.5	79.6	83.8	80.0
PCM	29.4	175.6	15.6	176.8	29.6	176.8	n.a.	n.a.	n.a.

T_{m1}, ΔH_{m1} = melting temperature and enthalpy (first heating scan); T_c, ΔH_c= crystallization temperature and enthalpy (cooling scan); T_{m2}, ΔH_{m2}= melting temperature and enthalpy (second heating scan); $\Delta H_{rel,m1}$, $\Delta H_{rel,c}$, $\Delta H_{rel,m2}$ = relative phase change enthalpy in the first heating, cooling, and second heating scans, respectively. n.a. = not applicable.

crystallization enthalpy values are always approx. 80 %, which indicates that the effective PCM weight fractions able to melt and crystallize are lower than the nominal values. This may be due to material remaining inside the beaker before mold casting, which advocates for an improvement in the foam preparation procedure.

During the first heating scan, all foam samples also exhibit a slight exothermic signal after 50 °C, which is absent during the second heating scan. This signal may be attributed to the residual crosslinking of polyurethane, suggesting that the foam production method could be optimized to obtain full curing from the onset. This was better investigated via DMTA (Figure S2,. Table S2), performed both on the as-produced foams and on samples treated at 200 °C for 30 min. The glass transition temperature, identified by the peak in the E'' signal, increases of up to 25 °C after the heat treatment, indicating the completion of the crosslinking and confirming the DSC findings.

DMTA tests also showed that the storage modulus starts decreasing from the early beginning of the thermal cycle, probably because of incomplete polymer crosslinking. Moreover, an additional small transition that only occurs in PCM-loaded samples can be attributed to the PCM melting. Also, for both as-produced and heat-treated samples, the values of E' in the PCM-containing samples are always higher than that of neat PU at 100 °C. This also occurs at 25 °C and 40 °C for PU-PCM10 and, only in the heat-treated case, for PUPCM20. Above PU's Tg, this is due to the presence of the microcapsules and, in particular, the capsule shell, which does not show any glass transition and acts as a rigid reinforcement in softening polyurethane. Below PU's Tg, this may be a sign of the contribution of the PCM to a higher crosslinking degree. Finally, in both non-treated and heat-treated cases, the addition of the PCM promotes a shift of the glass transition to higher temperatures and seems, therefore, to facilitate the process of crosslinking.

Although an increase in the PCM concentration increases the heat that can be stored and released by the foam, thereby enhancing the thermal buffering capabilities, it also detrimentally modifies the foam cell structure and decreases the volume fraction of closed cells, which diminishes the insulating capability of the foams. This is clear from the results of the HFM test, reported in Fig. 4. The thermal conductivity increases with the PCM content, from 0.024 W/(m·K) for neat PU to 0.037 W/(m·K) for PU-PCM30 at 10 °C, with the trends being confirmed

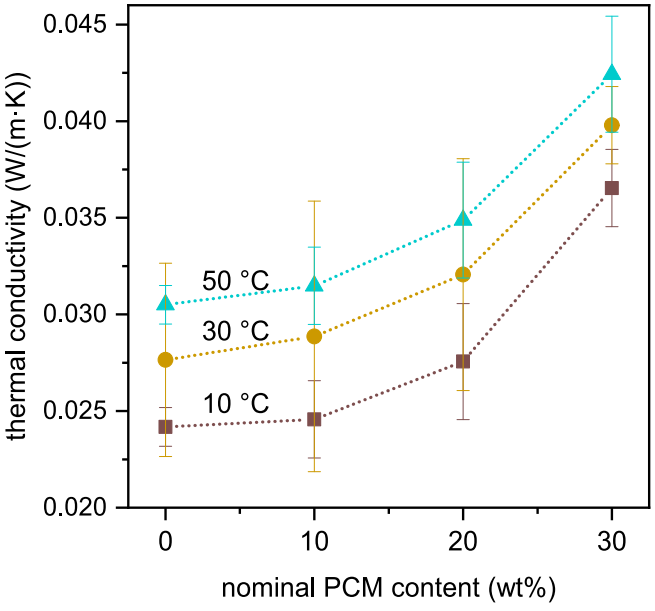

Fig. 4. Thermal conductivity of the prepared foam samples as a function of the nominal PCM concentration and the mean testing temperature.

at the other investigated temperatures. These results are similar to those found in the literature for similar PU/PCM systems [20,25]. More specifically, the increase in thermal conductivity is quite marginal up to a PCM content of 20 wt%, above which the increase is more significant. Given that the typical conductivity of insulating PU foams is 0.02–0.03 W/(m·K) [50,52–54], the thermal performance of PU-PCM30 samples could still be acceptable when leading to improved TES capabilities. In the end, the experimental results prove that, up to a nominal 30 wt% PCM addition, not only larger heat can be stored by PU foams but also the foam insulating capability may still be satisfactory. Hence, while the relatively low thermal conductivity may limit the rate of thermal energy storage and release, it provides valuable insulation properties, and the PCM's thermal inertia remains effective for temperature stabilization over the longer timescales typical of the intended applications.

The combination of the increased thermal buffering effect provided by the PCM, as investigated in DSC, and the increase in thermal conductivity, as measured via HFM, was studied on a larger scale via infrared thermography (Fig. 5a–d). The results of this test demonstrate that an increase in the PCM content prolongs the time required to reach the equilibrium temperature, both during heating and during cooling, due to the heat stored or released by the PCM during its phase transition. For instance, during heating to 50 °C, a nominal addition of 20 wt% PCM extends the time needed from 8 min of neat PU to 14 min of PU-PCM20. This is also evident by some of the camera frames recorded during the experiment, reported in Fig. 5a,b. Interestingly, for PU-PCM30 samples, the camera frames also reveal areas with different temperatures on the same surface, indicating zones with higher PCM concentrations and suggesting potential difficulties in homogeneously incorporating PCM microcapsules at such high PCM contents.

3.1.3. Mechanical properties of the foam samples

The flexural stress–strain curves recorded at 20 °C and 40 °C (Fig. 6a,

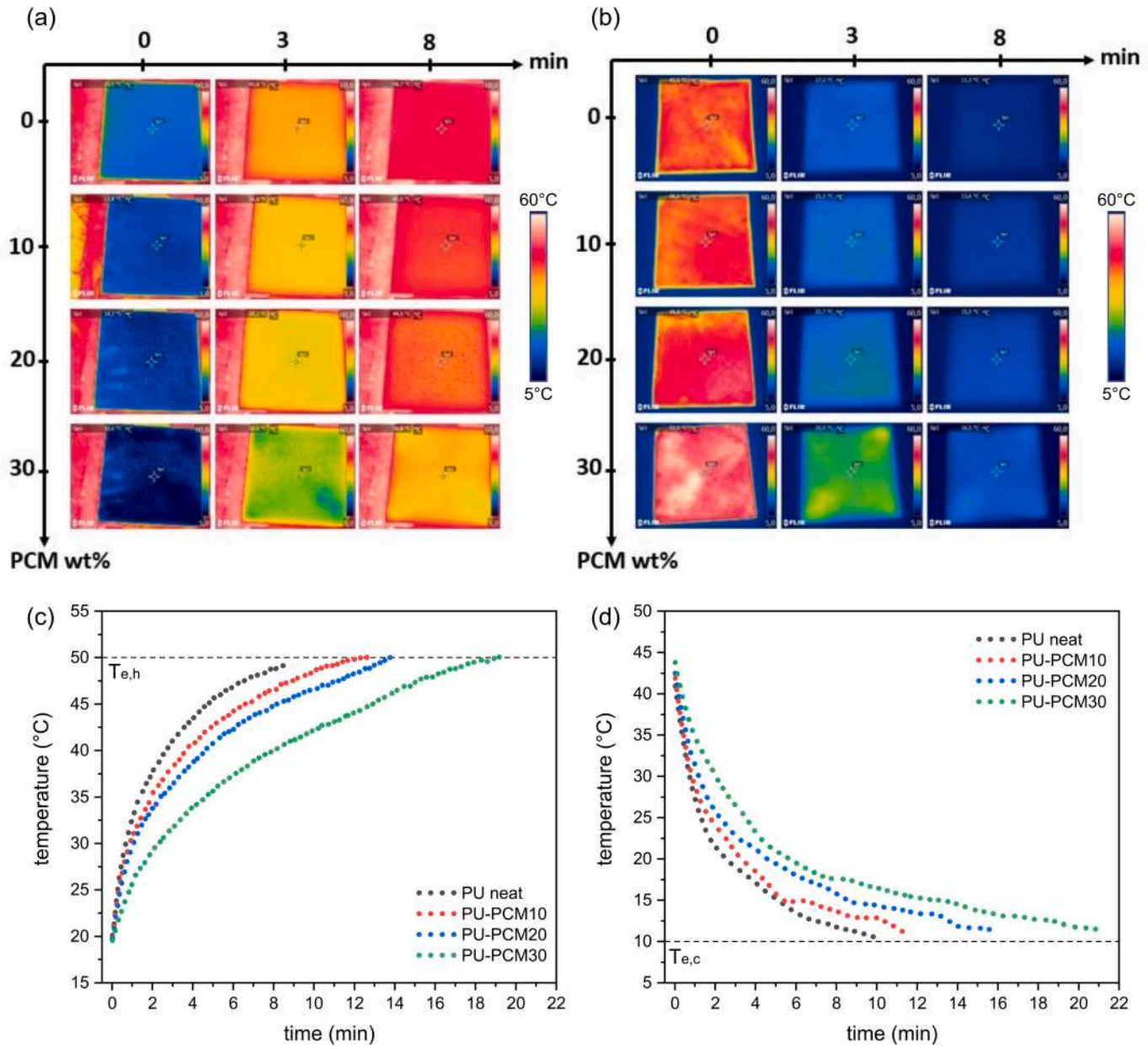

Fig. 5. Results of infrared thermography on foam samples. (a-b) Camera frames recorded at test start, after 3 min, and after 8 min as a function of the PCM nominal concentration in the heating (a) and cooling (b) experiments. (c-d) Temperature profiles of the foam surfaces (average temperature) as a function of time in the heating (c) and (d) cooling experiments. Te,h and Te,c indicate the environment temperature in the heating and cooling experiments, respectively.

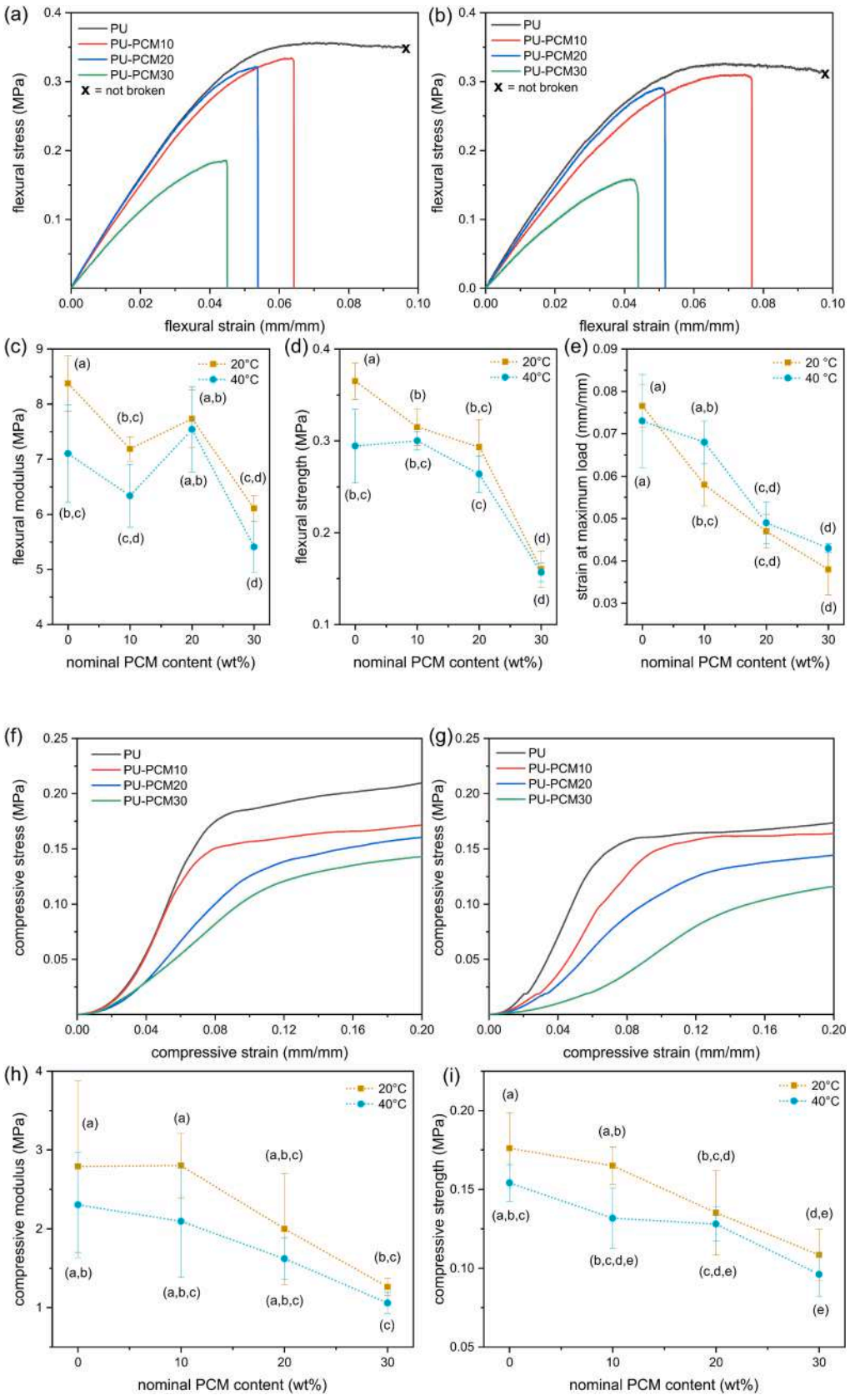

Fig. 6. Results of the mechanical characterization of the foam samples. (a-b) Representative stress–strain curves of the flexural tests performed at 20 °C (a) and at 40 °C (b). (c-e) Main results of the flexural tests; elastic modulus (c), flexural strength (d), and strain at maximum load (e) as a function of the PCM nominal concentration and the testing temperature. (f-g) Representative stress–strain curves of the compressive tests performed at 20 °C (f) and at 40 °C (g). (h-i) Main results of the compressive tests; compressive modulus (h), and compressive strength (i) as a function of the PCM nominal concentration and the testing temperature. Letters in brackets report the results of the Tukey's test after two-way ANOVA (same letter means no significant difference).

b) reveal that no fracture occurs for neat PU samples at either temperature. Instead, a continuously increasing vertical deflection is observed during measurement until the specimen starts slipping on the supports, at which point the test was interrupted. This phenomenon is not observed for the PCM-containing compositions, which all undergo fracture before starting to slip. Regarding the flexural modulus (Fig. 6c), as expected, the increase in temperature from 20 °C to 40 °C causes a decrease in stiffness. This occurs not only for PCM-containing samples but also for neat PU, indicating that the cause is not solely the PCM melting and confirming the incomplete curing of the polyurethane foams, in good agreement with DMTA results (see Figure S2). Moreover, up to a nominal PCM content of 20 wt%, the modulus remains almost constant, while it significantly decreases for samples containing 30 wt% PCM, with a maximum difference of 24 % compared to neat PU. Hence, the addition of up to 20 wt% PCM does not dramatically impair the foam modulus and provides satisfactory bending stiffness. Similar considerations can be made for the flexural strength (Fig. 6d): the maximum stress reached before failure is affected by the softening of non-cured polyurethane upon the temperature rise and remains almost constant for up to 20 wt% nominal PCM content. Furthermore, the flexural strain at maximum load (Fig. 6e) increases with temperature and decreases with PCM content due to the combined effects of thermal softening and cell structure modifications. These results are in good agreement with those found in the literature for similar systems [49].

The stress–strain curves under compressive loads (Fig. 6f,g) reveal that no yield point is observed in the samples, and the compressive stress continuously increases. Therefore, the stress value at 10 % strain is considered the compressive strength, and the values of the compressive modulus (E_c) and compressive strength (R_c) are calculated accordingly. As expected from the microstructural analysis, and similar to what has been reported in the literature [18,20,55], the compressive properties decrease with increasing PCM content. The cell opening effect promoted by the microcapsules, as well as the weakening and deformation of the existing cells, cause the reduction of both E_c (Fig. 6h) and R_c (Fig. 6i). The maximum decrease in compressive modulus between samples containing 30 wt% PCM and neat PU is approximately 55 %. On the contrary, the compressive strength decreases by a maximum of 39 % when adding a nominal 30 wt% PCM content, while the flexural strength shows a higher maximum drop of approximately 57 %. This suggests that the PCM primarily impairs the compressive stiffness and the flexural strength of the polyurethane-PCM foams. Regarding temperature and PCM melting, the modulus and strength seem to decrease with a temperature increase from 20 °C to 40 °C. However, all data are affected by a large deviation due to the non-homogeneous foam structure, and the two trends can be partially superimposed. Hence, molten PCM does not appear to significantly impair the compressive properties of the analyzed foams. Additionally, since the lower threshold of compressive strength for PU foams qualified to be used in load-bearing applications (e.g., in the building sector) is 0.1 MPa [26], all the produced foams are suitable for this application.

The comprehensive experimental investigation conducted on the different foam compositions led us to identify the most suitable PCM content able to provide TES functions without compromising excessively the thermal insulation capability, while also ensuring the necessary mechanical properties for structural applications and uses in sandwich panels. When added to PU foam, the PCM tends to be located inside the cell struts, promoting the weakening of the closed-cell structure in favor of an open-celled structure. Additionally, the higher the PCM weight fraction, the larger the thermal energy that can be stored in the foam, making it more suitable for TES applications, as appreciated with both DSC and thermal camera imaging. Moreover, while modifications occurring in the cell structure are responsible for a slight increase in thermal conductivity with PCM contents higher than 20 wt%, the foam remains a good thermal insulator even with a 30 wt% PCM content. Notably, the flexural properties are not significantly impaired up to a nominal 20 wt% PCM content, whereas the compressive properties are more affected by changes in the cell structure, suffering a reduction even with lower PCM contents. Consequently, the composition identified as the most suitable to produce sandwich composites is PU-PCM20, as it provides TES functions while guaranteeing low thermal conductivity and sufficiently good mechanical properties. In particular, the flexural behavior is primarily considered in the analysis, being less negatively affected than the compressive properties by PCM additions below 20 wt %. The results of the characterization of such composite sandwich panels with both neat PU and PU-PCM20 foam cores are presented hereafter.

3.2. Characterization of the sandwich panels

3.2.1. Microstructural properties of the sandwich panels

Light microscopy was performed on the sandwich panels especially to characterize the core-skin interface and examine the bonding area. As highlighted in the LM micrographs (Fig. 7a–d), the laminate bonds well with both neat PU and PU-PCM20 foam cores. A continuous adhesion is observed between the two materials, and no voids appear at the interface, revealing a very strong and defect-free interface, at least from the qualitative point of view. The presence of PCM microcapsules, visible as circular bright elements accumulated in the cell struts, (Fig. 7b), does not seem to diminish the interfacial adhesion. This is particularly noteworthy because these foams have undergone milling to remove the outermost dense skin and attain the desired foam thickness (see Section 2.2.2), which likely led to the exposure of more microcapsules on the foam surface. However, this did not affect the interfacial adhesion. This suggests that the epoxy/hardener mixture added to the foam during the hand layup process is effective in creating a strong and defect-free interface.

If the foam/laminate interface appears strong and defect-free, the laminates themselves contain some porosity, as indicated by red arrows in (Fig. 7a,b), which is certainly detrimental to their mechanical resistance. Such voids and defects are a direct consequence of the hand layup, which, although flexible and simple to perform, is associated with limitations that affect the final obtainable properties. For instance, the manual spread of the epoxy resin cannot guarantee that the reinforcement is homogeneously impregnated in all its parts and with the same amount of resin. Furthermore, if the vacuum is not properly applied or there is leakage, some air may remain trapped inside and generate voids and cavities in the resin. Hence, an automated resin impregnation, the autoclave process, or the use of prepregs could be potential solutions to reduce defects and improve the laminate quality.

3.2.2. Thermal characterization of the sandwich panels and calculation of the fiber volume fraction

The thermal characterization of the sandwich panels encompassed DSC and TGA tests on the epoxy/CF skins, performed to assess the curing protocol and calculate the fiber volume fraction, and the measurement of the thermal conductivity of the whole sandwich panels. A representative TGA thermogram of a laminate is presented in Figure S3, together with that of a specimen of neat epoxy resin. The degradation process of the epoxy/CF laminate is dominated by the degrading epoxy resin, while the fiber reinforcement remains in the final residuals. The main degradation step occurs at approx. 350 °C for both the laminate and the resin, proceeding with its maximum rate at approx. 375 °C (Table S3). The laminate residue ($m_{R,700} \sim 67$ %) is mainly represented by carbon fibers but also contains a small fraction of epoxy resin, for which $m_{R,700}$ is around 5 %. Such data were used to determine a fiber volume fraction of 57 $\pm$ 2 vol%, with no significant differences between the laminate specimens taken from the S-PU samples and those taken from S-PU-PCM20 samples. This value is close to that calculated via the weighing method (see Section 2.3.1), equal to 60 $\pm$ 2 vol%, which is slightly higher probably because the initial assumption of no porosity is not fully correct, as the LM micrographs demonstrate. Nevertheless, the closeness of the two values suggests that the porosity in the laminates is relatively small and that the fiber reinforcement is homogeneously distributed in

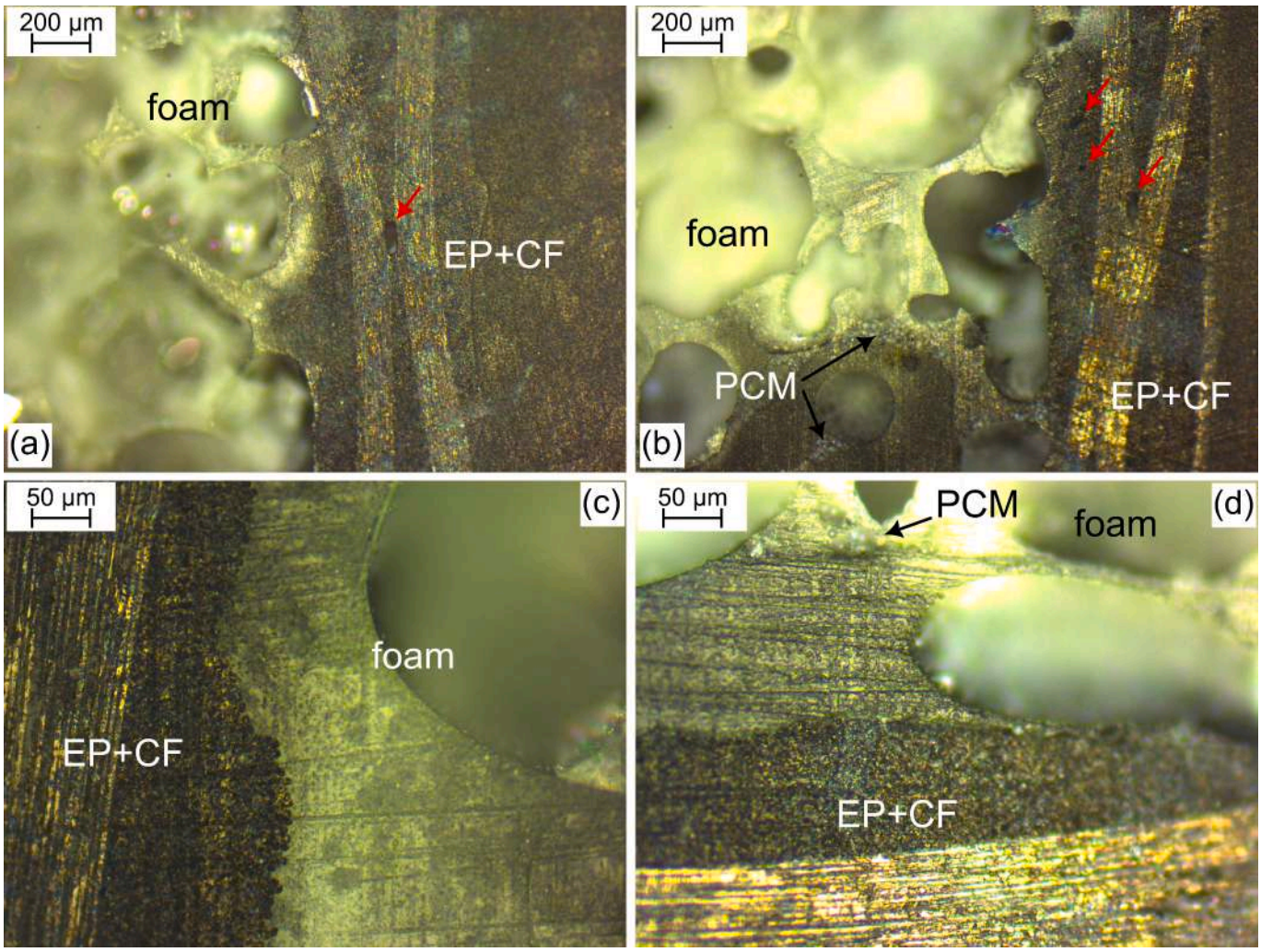

Fig. 7. Light microscope images of the polished cross-section of the sandwich samples, highlighting the interfacial adhesion. Low (a) and high (c) magnification micrograph of S-PU sample. Red arrows indicate porosity in the epoxy/CF laminate; low (b) and high (d) magnification micrograph of the S-PU-PCM20 sample.

the epoxy matrix, making the TGA results representative of the entire laminate. The calculated fiber volume fraction is typical of traditional epoxy/carbon laminates for structural purposes [56,57] and leads to the desired mechanical properties for the sandwich structure.

The DSC thermograms of the composite laminate during the first heating, cooling, and second heating scans (Figure S4) do not show any exothermic peaks associated with residual crosslinking, indicating that the curing parameters selected in sample preparation were suitable and effective in producing a composite laminate with the desired properties. The T_g, equal to 75 °C in the first heating scan, increases in the second heating scan as a result of further curing the epoxy receives during the test. In any case, the value obtained from the first heating scan is in accordance with the target property value indicated by the resin producer and well above the target service temperature of these laminates (20–50 °C).

Among the most significant thermal properties of the prepared laminates is thermal conductivity. The values for the thermal conductivity at 10 °C, 30 °C, and 50 °C (Table 3) show that the addition of two composite laminate skins does not seem to impair the thermal insulation properties of the foam material, as the thermal conductivity does not increase significantly compared to that measured on the skins after milling. A growth in thermal conductivity would have been detected if the epoxy resin had penetrated the foam pores, replacing the poor conductive gas inside them, but this does not seem to be the case. Similar to the analysis of foam samples, the sample containing the microcapsules shows a slightly higher thermal conductivity than the neat sample in all temperature conditions. Thus, the produced sandwich panels preserve both the thermal energy storage and insulation properties that characterize the chosen foam composition. Finally, the data suggest that the operations for preparing the sandwich foam cores played a role in increasing the thermal conductivity of the foam material, with foam milling believed to be the main factor responsible for locally damaging the foam cell structure.

Table 3
HFM thermal conductivity of the prepared sandwich samples and the relative foam core samples after milling, evaluated at 10 °C, 30 °C, and 50 °C.

Sample		$\lambda_{10°C}$(W/(m·K))	$\lambda_{30°C}$(W/(m·K))	$\lambda_{50°C}$(W/(m·K))
Foams	PU	0.031 ± 0.001	0.034 ± 0.001	0.037 ± 0.001
	PU-PCM20	0.033 ± 0.001	0.036 ± 0.001	0.039 ± 0.001
Sandwich panels	S-PU	0.032 ± 0.001	0.035 ± 0.001	0.038 ± 0.002
	S-PU-PCM20	0.036 ± 0.002	0.04 ± 0.002	0.043 ± 0.002

3.2.3. *Mechanical characterization of the sandwich panels*

The mechanical characterization of the prepared sandwich panels

encompassed three-point flexural, edgewise compression, and flatwise tensile tests, and the results of this extensive characterization are reported in Figs. 8-11. For flexural tests, the flexural load–displacement curves (Fig. 8a) are characterized by a linear load–displacement relationship in the initial part, with a progressively decreasing slope in the region preceding the maximum load. At the maximum load, the behavior differs between neat S-PU and S-PU-PCM20 panels. In PCM-containing specimens, failure occurs in two steps: the load drops suddenly after reaching its maximum but then increases again until the second drop. For specimens with a neat PU foam core, the load plateaus and then suddenly drops to zero at much higher displacement values. This difference underlines a different failure mechanism. The sudden load drop in the S-PU specimens core is associated with the top face sheet failure at the contact point with the test fixture, due to the compression-induced local bending of the skin (Fig. 8b) [58,59]. Conversely, the process observed for S-PU-PCM20 is characterized by a shear failure in the sandwich core, originating in the center foam thickness and propagating diagonally to the face sheets, followed by the bottom facing separating from the core (Fig. 8c). No failure begins from the interfacial bonding between the foam core and the outer face sheets, confirming good adhesion at the core-skin interface. Since the maximum load reached during the test is comparable across the compositions, the calculated core shear ultimate strength and facing stress values, reported in Fig. 11a, are only slightly impaired by the PCM and are comparable to values found in the literature for structural sandwich panels [59]. However, since the main failure mechanism for S-PU-PCM20 samples is the shear failure of the foam core, future work might involve the improvement of the foam's shear resistance.

The representative load–displacement curves of the edgewise compression tests (Fig. 9a) show that the maximum load reached by the PCM-containing sample is significantly lower than that reported for the neat S-PU sample. After the first failure, the load drops gradually with increasing displacement until it stabilizes to a plateau value, which represents the residual mechanical resistance. When reloading the specimens (Fig. 9b), the maximum load never exceeds that stabilization load value. For the neat S-PU sample, the load starts increasing again only after a certain displacement, indicating residual deformation after failure. This effect is less evident in S-PU-PCM20 specimens, as they experience limited deflection and reach failure sooner when the load is applied for the first time.

The calculated edgewise compressive strength values (σ_{ec}^{ult}) (Fig. 11b) of S-PU-PCM20 are lower (–30 %) than those of neat S-PU. This result is expected given the decreasing trend of compressive properties with increasing PCM content observed for the foams. However, the compressive strength of neat PU and PCM-containing samples is determined by different failure mechanisms. For neat PU specimens, failure is caused by the face sheet fracturing under compression after buckling of the entire sandwich structure (Fig. 11c). This damage mechanism, known as overall column buckling, has been extensively studied and reported as one of the most common collapse modes for sandwich structures [60]. When further loading the damaged specimen, the flexural rigidity progressively decreases until the other skin fractures under tension (Fig. 11d), with the foam core bending extensively and suffering internal shear damage. In contrast, PCM-containing specimens undergo unstable sandwich disintegration [60] with buckling of face sheets in opposite directions. The applied load causes the buckling of either one or both face sheets towards the outside, as the tensile strength of the foam core at the core-skin interface is insufficient to hold the facings bonded together (Fig. 11e,f). A layer of foam material remains adherent to the detached facing, indicating cohesive foam failure and good interface adhesion. The foam core fails at mid-height where the bending load is more intense and propagates rapidly parallel to the face sheets.

Finally, the results of the flatwise tensile tests are reported in Fig. 10a–c. The representative load–displacement curves (Fig. 10a) show a similar trend for both compositions: initially, the load increases slowly, and then the slope increases as the load rises continuously with displacement until failure. Again, the maximum load reached by neat PU specimens is higher than that of PCM-containing specimens, and a similar tendency occurs for the ultimate flatwise tensile strength (σ_t^{ult}, Fig. 11c), which drops from 362 kPa of S-PU to 207 kPa of S-PU-PCM20 and is seen depending primarily on the tensile strength of the foam core. Such decreasing trend of the σ_t^{ult} upon PCM addition was expected based on the microstructural and mechanical analysis of the foam materials. However, considering the typical purpose of sandwich structures, an out-of-plane tensile load is unlikely to be applied during normal use, and thus the reduced tensile strength of the PCM-containing sample is not a primary issue. More significantly, a cohesive fracture of the foam core occurred in all tests, regardless of the presence of PCM (Fig. 10b,c), indicating that the adopted production process was very effective in realizing optimal adhesion between the laminates and the foam core.

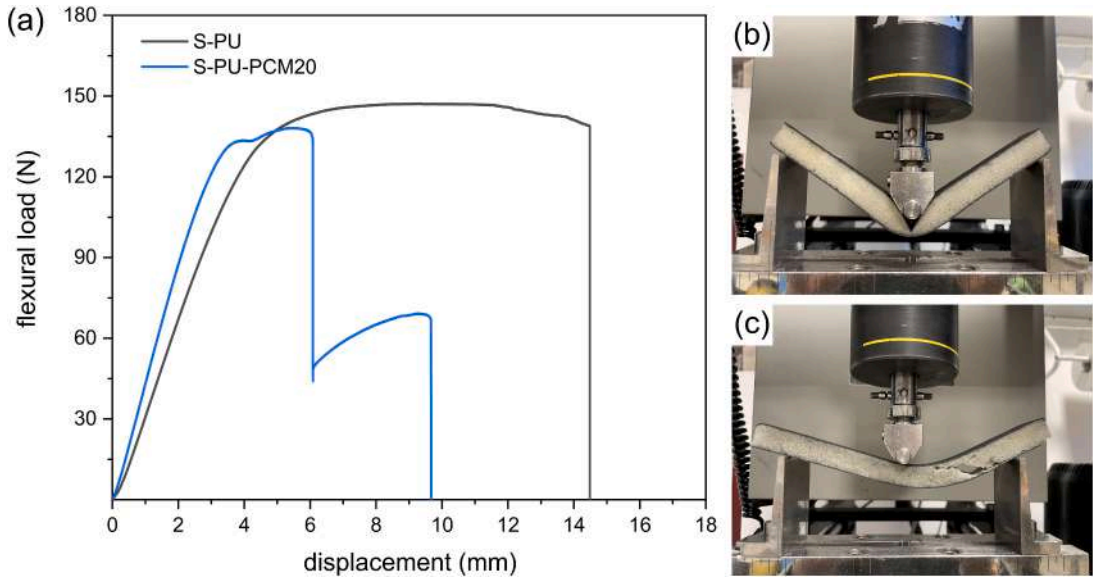

Fig. 8. (a) Representative load–displacement curves obtained from flexural tests of sandwich samples. (b) outer facing failure for S-PU specimens; (c) foam core shear failure for S-PU-PCM20 specimens.

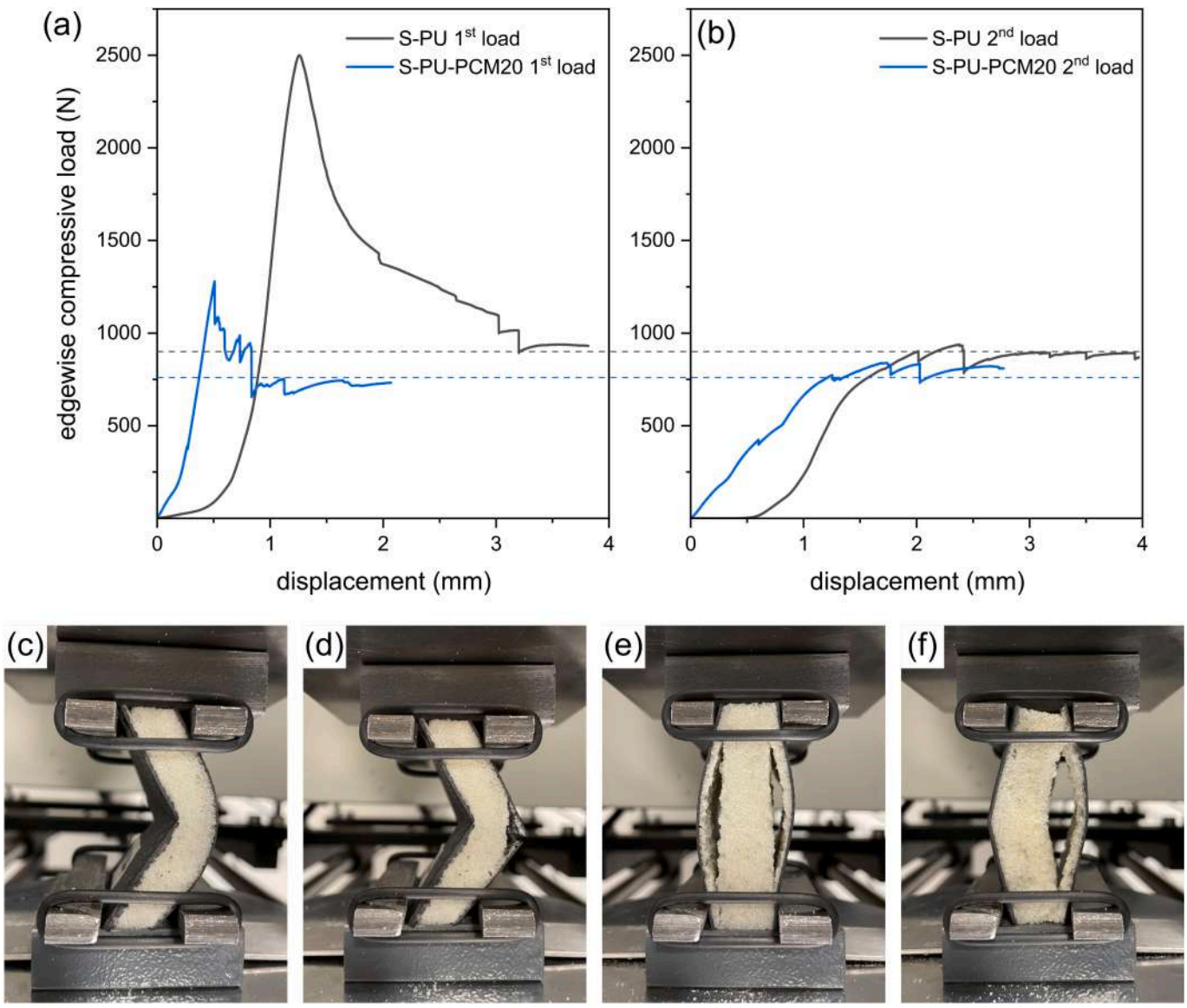

Fig. 9. Results of the edgewise compression tests on the prepared sandwich samples. (a) Representative load–displacement curves during the first loading; (b) load–displacement behavior of samples after the first failure. The dashed line represents the maximum load observed for reloaded samples, which is comparable to the load value at stabilization after the first failure. S-PU specimens show overall column buckling as the preferred failure mode: (c) compressive fracture of the left facing, and (d) tensile fracture of the right facing after prolonged application of the load. S-PU-PCM20 specimens show sandwich disintegration with buckling of the outer facings: (e) only one skin is separated from the foam core, and (f) both skins are debonded.

4. Conclusions

This work successfully developed and comprehensively characterized novel multifunctional sandwich composites that synergistically integrate structural load-bearing capability with thermal management properties. These composites combined PU foam cores containing microencapsulated PCMs with high-performance epoxy/carbon fiber laminate skins. Such materials show promise for applications demanding lightweight yet robust thermoregulating composites like refrigerated transportation, aerospace, and automotive industries.

First, the systematic investigation of PU/PCM foams with up to 30 wt % PCM revealed an optimized PU foam composition with 20 wt% PCM content. While higher PCM loadings enhanced thermal buffering from latent heat storage, they promoted a detrimental closed-to-open cell transition that severely compromised thermal insulation and mechanical properties. The 20 wt% PU-PCM foam (sample PU-PCM20) provided a balanced combination of adequate thermal energy storage (up to 29 J/g) and low thermal conductivity (0.032 W/(m·K) at 30 °C), while maintaining satisfactory flexural and compressive properties.

Sandwich panels produced with this optimized PU-PCM20 foam core exhibited good structural integrity and interfacial adhesion between the foam core and carbon/epoxy laminate skins. Light microscopy revealed a continuous, defect-free bonding at the core-skin interface with no evidence of voids or delamination. This excellent interfacial adhesion enabled the sandwich panels to withstand flexural, edgewise compression, and flatwise tensile loading conditions characteristic of structural applications. Under three-point flexural loading, the PCM-containing panels achieved comparable core shear strengths of 149 kPa and facing stresses of 25 MPa relative to neat PU sandwich controls. However, the edgewise compressive strength was approx. 30 % lower at 30 MPa for PU-PCM20 panels due to premature unstable disintegration from core shear failure rather than overall buckling seen in neat samples, and the flatwise tensile strength also suffered from a significant decrease, dropping to 207 kPa (−42 % than neat S-PU sandwich).

In summary, this study demonstrated the feasibility of realizing multifunctional composites with simultaneous load-bearing and thermal

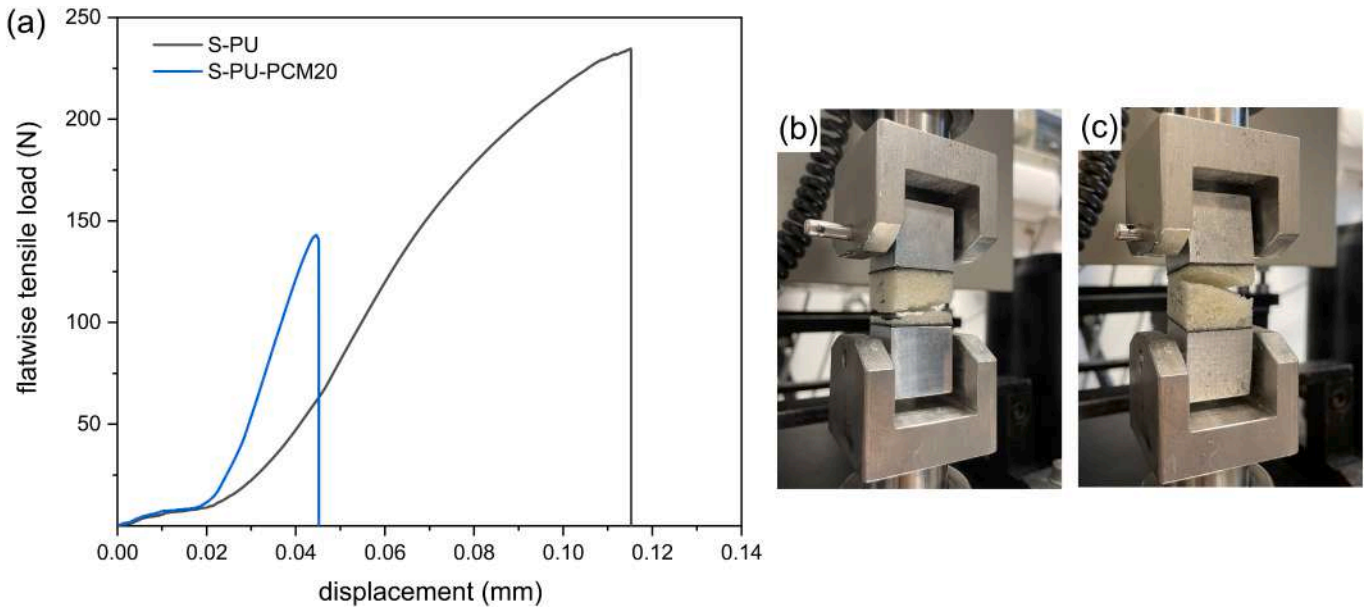

Fig. 10. Results of the flatwise tensile tests on the prepared sandwich samples. (a) Representative load–displacement curves. For both S-PU (b) and S-PU-PCM20 (c), failure occurs due to core fracturing.

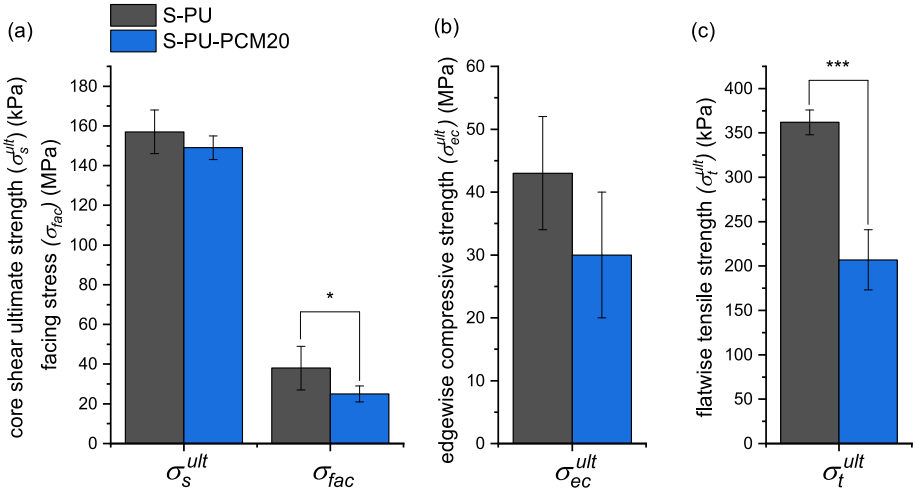

Fig. 11. Summary of the results of the mechanical properties of the prepared sandwich panels. (a) results of the three-point bending tests (σ_s^{ult} = core shear ultimate strength; σ_{fac} = facing stress); (b) results of the edgewise compression tests (σ_{ec}^{ult} = ultimate edgewise compressive strength); (c) results of the flatwise tensile tests (σ_t^{ult} = ultimate flatwise tensile strength). Asterisks indicate statistically significant differences according to one-way ANOVA test (p-value = 0 '***' 0.001 '**' 0.01 '*' 0.05).

regulation capabilities by judiciously incorporating PCMs within the sandwich foam core architecture. These multifunctional sandwich composites have significant potential in various industries. In refrigerated transportation, they could be used to construct truck trailers or shipping containers, providing both structural integrity and improved temperature stability for sensitive cargo. In aerospace applications, these materials could be utilized in aircraft cabin panels or cargo holds, offering weight savings while enhancing thermal comfort and energy efficiency. For the automotive industry, they could be employed in electric vehicle battery enclosures, helping to maintain optimal battery temperature while providing structural support. These promising results highlight the possibility of tailoring this concept towards specific applications by further characterizing and improving the shear response of PCM-modified foams through proper additives. Exploring alternative core materials and PCM types also presents opportunities to further optimize these multifunctional composite systems to tailor the composites for specific application environments. Finally, scaling up the production process and conducting full-scale prototyping would be essential steps towards commercialization and real-world implementation of these multifunctional composites.

Funding

This research activity has been supported by the Air Force Office of Scientific Research (AFOSR) within the project "Multifunctional polymer composites for thermal energy storage: current trends and future perspectives", Grant Number: FA8655-23–1-7039.

CRediT authorship contribution statement

Giulia Fredi: Writing – review & editing, Writing – original draft, Visualization, Supervision, Methodology, Funding acquisition, Formal

analysis, Data curation, Conceptualization. **Elisa Boso:** Writing – review & editing, Visualization, Investigation. **Alessandro Sorze:** Writing – review & editing, Supervision, Resources, Project administration, Funding acquisition. **Alessandro Pegoretti:** Writing – review & editing, Supervision, Resources, Project administration, Funding acquisition.

Declaration of competing interest

The authors declare the following financial interests/personal relationships which may be considered as potential competing interests: [Alessandro Pegoretti reports financial support was provided by Air Force Office of Scientific Research. If there are other authors, they declare that they have no known competing financial interests or personal relationships that could have appeared to influence the work reported in this paper].

Data availability

Data will be made available on request.

Acknowledgments

Elantas Europe Srl (Parma, Italy) is gratefully acknowledged for providing the employed epoxy system. Mr. Davide Perin is gratefully acknowledged for his assistance during the preparation of the laminates.

Appendix A. Supplementary data

Supplementary data to this article can be found online at https://doi.org/10.1016/j.compositesa.2024.108382.

References

[1] Corigliano A, Rizzi E, Papa E. Experimental characterization and numerical simulations of a syntactic-foam/glass-fibre composite sandwich. Compos Sci Technol 2000;60:2169–80.
[2] Pareta AS, Gupta R, Panda SK. Experimental investigation on fly ash particulate reinforcement for property enhancement of PU foam core FRP sandwich composites. Composites Science and Technology 2020:195. https://doi.org/10.1016/j.compscitech.2020.108207.
[3] Kausar A, Ahmad I, Rakha SA, Eisa MH, Diallo A. State-of-the-art of sandwich composite structures: manufacturing—to—high performance applications. Journal of Composites Science 2023;7(3). https://doi.org/10.3390/jcs7030102.
[4] Kausar A. Polyurethane composite foams in high-performance applications: a review. Polym-Plast Technol Eng 2017;57(4):346–69. https://doi.org/10.1080/03602559.2017.1329433.
[5] Castellón C, Medrano M, Roca J, Cabeza LF, Navarro ME, Fernández AI, et al. Effect of microencapsulated phase change material in sandwich panels. Renew Energy 2010;35(10):2370–4. https://doi.org/10.1016/j.renene.2010.03.030.
[6] Hasse C, Grenet M, Bontemps A, Dendievel R, Sallée H. Realization, test and modelling of honeycomb wallboards containing a phase change material. Energ Buildings 2011;43(1):232–8. https://doi.org/10.1016/j.enbuild.2010.09.017.
[7] Jia Z, Hu C, Zhang Y, Zhang S, Tang B. Exploring electro-thermal conversion in phase change materials: a review. Compos A Appl Sci Manuf 2023:175. https://doi.org/10.1016/j.compositesa.2023.107809.
[8] Pielichowska K, Pielichowski K. Phase change materials for thermal energy storage. Prog Mater Sci 2014;65:67–123. https://doi.org/10.1016/j.pmatsci.2014.03.005.
[9] Yadav M, Pasarkar N, Naikwadi A, Mahanwar P. A review on microencapsulation, thermal energy storage applications, thermal conductivity and modification of polymeric phase change material for thermal energy storage applications. Polym Bull 2022;80(6):5897–927. https://doi.org/10.1007/s00289-022-04369-x.
[10] Khadiran T, Hussein MZ, Zainal Z, Rusli R. Encapsulation techniques for organic phase change materials as thermal energy storage medium: a review. Sol Energy Mater Sol Cells 2015;143:78–98. https://doi.org/10.1016/j.solmat.2015.06.039.
[11] Giro-Paloma J, Martínez M, Cabeza LF, Fernández AI. Types, methods, techniques, and applications for microencapsulated phase change materials (MPCM): a review. Renew Sustain Energy Rev 2016;53:1059–75. https://doi.org/10.1016/j.rser.2015.09.040.
[12] Li Z, Zhang Y, Wang X, Cao F, Zhang S, Tang B. Composite phase change materials with room-temperature-flexibility. Compos A Appl Sci Manuf 2024:182. https://doi.org/10.1016/j.compositesa.2024.108173.
[13] Palacios A, Navarro-Rivero ME, Zou B, Jiang Z, Harrison MT, Ding Y. A perspective on phase change material encapsulation: guidance for encapsulation design methodology from low to high-temperature thermal energy storage applications. J Storage Mater 2023:72. https://doi.org/10.1016/j.est.2023.108597.
[14] Fu T, Wang W, Fang G. Thermal properties and applications of form-stable phase change materials for thermal energy storage and thermal management: a review. Energy Storage 2023;6(1). https://doi.org/10.1002/est2.533.
[15] Cheng H, Han G, Su M, He C, Liu C, Feng Y. Silver nanowire bridged graphene framework for encapsulating phase change materials with high thermal conductivity and solar-to-heat conversion ability. Compos A Appl Sci Manuf 2024:182. https://doi.org/10.1016/j.compositesa.2024.108207.
[16] Marani A, Madhkhan M. An innovative apparatus for simulating daily temperature for investigating thermal performance of wallboards incorporating PCMs. Energ Buildings 2018;167:1–7. https://doi.org/10.1016/j.enbuild.2018.02.029.
[17] Sukontasukkul P, Sangpet T, Newlands M, Tangchirapat W, Limkatanyu S, Chindaprasirt P. Thermal behaviour of concrete sandwich panels incorporating phase change material. Adv Build Energy Res 2020;16(1):64–88. https://doi.org/10.1080/17512549.2020.1788990.
[18] Mahajan UR, Emmanuel I, Rao AS, Mhaske ST. Development of rigid polyurethane foam incorporating phase change material for a low-temperature thermal energy storage application. Polym Int 2023;72(5):490–9. https://doi.org/10.1002/pi.6492.
[19] Nandy A, Houl Y, Zhao W, D'Souza NA. Thermal heat transfer and energy modeling through incorporation of phase change materials (PCMs) into polyurethane foam. Renew Sustain Energy Rev 2023:182. https://doi.org/10.1016/j.rser.2023.113410.
[20] Vatankhah E, Abasnezhad M, Nazerian M, Barmar M, Partovinia A. Thermal energy storage and mechanical performance of composites of rigid polyurethane foam and phase change material prepared by one-shot synthesis method. J Polym Res 2022;29(3). https://doi.org/10.1007/s10965-022-02911-z.
[21] Sarkar S, Mestry S, Mhaske ST. Developments in phase change material (PCM) doped energy efficient polyurethane (PU) foam for perishable food cold-storage applications: a review. J Storage Mater 2022:50. https://doi.org/10.1016/j.est.2022.104620.
[22] Naikwadi AT, Samui AB, Mahanwar PA. Fabrication and experimental investigation of microencapsulated eutectic phase change material-integrated polyurethane sandwich tin panel composite for thermal energy storage in buildings. Int J Energy Res 2021;45(15):20783–94. https://doi.org/10.1002/er.7138.
[23] Ikutegbe CA, Farid MM. Application of phase change material foam composites in the built environment: a critical review. Renew Sustain Energy Rev 2020:131. https://doi.org/10.1016/j.rser.2020.110008.
[24] Amaral C, Pinto SC, Silva T, Mohseni F, Amaral JS, Amaral VS, et al. Development of polyurethane foam incorporating phase change material for thermal energy storage. J Storage Mater 2020:28. https://doi.org/10.1016/j.est.2019.101177.
[25] Amaral C, Vicente R, Ferreira VM, Silva T. Polyurethane foams with microencapsulated phase change material: comparative analysis of thermal conductivity characterization approaches. Energ Buildings 2017;153:392–402. https://doi.org/10.1016/j.enbuild.2017.08.019.
[26] Yang C, Fischer L, Maranda S, Worlitschek J. Rigid polyurethane foams incorporated with phase change materials: a state-of-the-art review and future research pathways. Energ Buildings 2015;87:25–36. https://doi.org/10.1016/j.enbuild.2014.10.075.
[27] Galvagnini F, Dorigato A, Valentini F, Fiore V, La Gennusa M, Pegoretti A. Multifunctional polyurethane foams with thermal energy storage/release capability. J Therm Anal Calorim 2020;147(1):297–313. https://doi.org/10.1007/s10973-020-10367-w.
[28] Fioretti R, Principi P, Copertaro B. A refrigerated container envelope with a PCM (Phase Change Material) layer: experimental and theoretical investigation in a representative town in Central Italy. Energ Conver Manage 2016;122:131–41. https://doi.org/10.1016/j.enconman.2016.05.071.
[29] Konuklu Y, Paksoy HÖ. Phase change material sandwich panels for managing solar gain in buildings. J Sol Energy Eng 2009;131:041012. https://doi.org/10.1115/1.3197839.
[30] Dębska B, Lichołai L, Szyszka J. Innovative composite on the basis of an aerogel mat with an epoxy resin modified with PET waste and PCM. E3S Web of Conferences 2018:44. https://doi.org/10.1051/e3sconf/20184400031.
[31] Fredi G, Dorigato A, Fambri L, Pegoretti A. Multifunctional structural composites for thermal energy storage. Multifunctional Materials 2020;3:042001. https://doi.org/10.1088/2399-7532/abc60c.
[32] Fredi G, Dorigato A, Fambri L, Pegoretti A. Evaluating the multifunctional performance of structural composites for thermal energy storage. Polymers 2021;13(18):3108. https://doi.org/10.3390/polym13183108.
[33] Su J-F, Zhao Y-H, Wang X-Y, Dong H, Wang S-B. Effect of interface debonding on the thermal conductivity of microencapsulated-paraffin filled epoxy matrix composites. Composites Part A: Applied Science and Manufacturing 2012;43(3):325–32. https://doi.org/10.1016/j.compositesa.2011.12.003.
[34] Fredi G, Dorigato A, Fambri L, Pegoretti A. Multifunctional epoxy/carbon fiber laminates for thermal energy storage and release. Compos Sci Technol 2018;158:101–11. https://doi.org/10.1016/j.compscitech.2018.02.005.
[35] Fredi G, Dorigato A, Unterberger S, Artuso N, Pegoretti A. Discontinuous carbon fiber/polyamide composites with microencapsulated paraffin for thermal energy storage. J Appl Polym Sci 2019;136(16). https://doi.org/10.1002/app.47408.
[36] Galvagnini F, Fredi G, Dorigato A, Fambri L, Pegoretti A. Mechanical behaviour of multifunctional epoxy/hollow glass microspheres/paraffin microcapsules syntactic foams for thermal management. Polymers 2021;13(17):2896. https://doi.org/10.3390/polym13172896.
[37] Dorigato A, Fredi G, Negri M, Pegoretti A. Thermo-mechanical behaviour of novel wood laminae-thermoplastic starch biodegradable composites with thermal energy

storage/release capability. Front Mater 2019;6:1–12. https://doi.org/10.3389/fmats.2019.00076.
[38] Umate TB, Sawarkar PD. A review on thermal energy storage using phase change materials for refrigerated trucks: active and passive approaches. J Storage Mater 2024;75. https://doi.org/10.1016/j.est.2023.109704.
[39] Selvnes H, Allouche Y, Manescu RI, Hafner A. Review on cold thermal energy storage applied to refrigeration systems using phase change materials. Thermal Science and Engineering Progress 2021;22. https://doi.org/10.1016/j.tsep.2020.100807.
[40] Roy A, Kale S, Lingayat AB, Sur A, Arun S, Sengar D, et al. Evaluating energy-saving potential in micro-cold storage units integrated with phase change material. J Braz Soc Mech Sci Eng 2023;45(10). https://doi.org/10.1007/s40430-023-04434-0.
[41] Kuhn J, Ebert HP, Arduini-Schuster MC, Buttner D, Fricke J. Thermal transport in polystyrene and polyurethane foam insulations. Int J Heat Mass Transfer 1992;35(7):1795.
[42] Serrano A, Borreguero AM, Garrido I, Rodríguez JF, Carmona M. The role of microstructure on the mechanical properties of polyurethane foams containing thermoregulating microcapsules. Polym Test 2017;60:274–82. https://doi.org/10.1016/j.polymertesting.2017.04.011.
[43] Fredi G, Simon F, Sychev D, Melnyk I, Janke A, Scheffler C, et al. Bioinspired polydopamine coating as an adhesion enhancer between paraffin microcapsules and an epoxy matrix. ACS Omega 2020;5:19639–53. https://doi.org/10.1021/acsomega.0c02271.
[44] Fredi G, Zimmerer C, Scheffler C, Pegoretti A. Polydopamine-coated paraffin microcapsules as a multifunctional filler enhancing thermal and mechanical performance of a flexible epoxy resin. Journal of Composites Science 2020;4(4):174. https://doi.org/10.3390/jcs4040174.
[45] Zimmerer C, Fredi G, Putzke S, Boldt R, Janke A, Krause B, et al. Dopamine as a bioinspired adhesion promoter for the metallization of multi-responsive phase change microcapsules. J Mater Sci 2022;57:16755–75. https://doi.org/10.1007/s10853-022-07658-y.
[46] Fredi G, Dorigato A, Pegoretti A. Dynamic-mechanical response of carbon fiber laminates with a reactive thermoplastic resin containing phase change microcapsules. Mechanics of Time-Dependent Materials 2020;24(3):395–418. https://doi.org/10.1007/s11043-019-09427-y.
[47] Fredi G, Dorigato A, Fambri L, Pegoretti A. (2020) Detailed experimental and theoretical investigation of the thermo-mechanical properties of epoxy composites containing paraffin microcapsules for thermal management Polymer Engineering and Science. 60:1202–20. DOI: 10.1002/PEN.25374.
[48] Gaidukovs S, Gaidukova G, Ivdre A, Cabulis U. Viscoelastic and thermal properties of polyurethane foams obtained from renewable and recyclable components. J Renewable Mater 2018. https://doi.org/10.7569/jrm.2018.634112.
[49] You M, Zhang X-x, Wang X-c, Zhang L, Wen W. Effects of type and contents of microencapsuled n-alkanes on properties of soft polyurethane foams. Thermochimica Acta 2010;500(1–2):69–75. https://doi.org/10.1016/j.tca.2009.12.013.
[50] Berardi U. The impact of aging and environmental conditions on the effective thermal conductivity of several foam materials. Energy 2019;182:777–94. https://doi.org/10.1016/j.energy.2019.06.022.
[51] Zhang XX, Fan YF, Tao XM, Yick KL. Crystallization and prevention of supercooling of microencapsulated n-alkanes. J Colloid Interface Sci 2005;281(2):299–306. https://doi.org/10.1016/j.jcis.2004.08.046.
[52] Gama NV, Ferreira A, Barros-Timmons A. Polyurethane foams: past, present, and future. Materials (Basel) 2018;11(10). https://doi.org/10.3390/ma11101841.
[53] Kabakci E, Sayer G, Suvaci E, Uysal O, Güler İ, Kaya M. Processing-structure-property relationship in rigid polyurethane foams. J Appl Polym Sci 2017;134(21). https://doi.org/10.1002/app.44870.
[54] Zhang H, Fang W-Z, Li Y-M, Tao W-Q. Experimental study of the thermal conductivity of polyurethane foams. Appl Therm Eng 2017;115:528–38. https://doi.org/10.1016/j.applthermaleng.2016.12.057.
[55] Mane JV, Chandra S, Sharma S, Ali H, Chavan VM, Manjunath BS, et al. Mechanical property evaluation of polyurethane foam under quasi-static and dynamic strain rates- an experimental study. Procedia Engineering 2017;173:726–31. https://doi.org/10.1016/j.proeng.2016.12.160.
[56] Brunbauer J, Stadler H, Pinter G. Mechanical properties, fatigue damage and microstructure of carbon/epoxy laminates depending on fibre volume content. Int J Fatigue 2015;70:85–92. https://doi.org/10.1016/j.ijfatigue.2014.08.007.
[57] Ansari MTA, Singh KK, Azam MS. Fatigue damage analysis of fiber-reinforced polymer composites—a review. J Reinf Plast Compos 2018;37(9):636–54. https://doi.org/10.1177/0731684418754713.
[58] Steeves CA, Fleck NA. Collapse mechanisms of sandwich beams with composite faces and a foam core, loaded in three-point bending. Part II: experimental investigation and numerical modelling. Int J Mech Sci 2004;46(4):585–608. https://doi.org/10.1016/j.ijmecsci.2004.04.004.
[59] Junaedi H, Khan T, Sebaey TA. Characteristics of carbon-fiber-reinforced polymer face sheet and glass-fiber-reinforced rigid polyurethane foam sandwich structures under flexural and compression tests. Materials (Basel) 2023;16(14). https://doi.org/10.3390/ma16145101.
[60] Mamalis AG, Manolakos DE, Ioannidis MB, Papapostolou DP. On the crushing response of composite sandwich panels subjected to edgewise compression: experimental. Compos Struct 2005;71(2):246–57. https://doi.org/10.1016/j.compstruct.2004.10.006.